doi.org/10.1002/batt.201900221

Construction of Hierarchical 2D PANI/Ni_3S_2 Nanosheet Arrays on Ni Foam for High-Performance Asymmetric Supercapacitors

Qiuhui Cheng,[a] Cui Yang,*[b] Lei Han,*[a, c, d] and Kai Tao*[a, c, d]

In this work, a hierarchical 2D polyaniline (PANI)/Ni_3S_2 nanosheet arrays on Ni foam (NF) with open network was successfully developed by the growth of Ni_3S_2 nanosheet arrays derived from 2D Ni–MOF templates followed by the electrodeposition of a layer of PANI nanoflakes. The as-prepared PANI/Ni_3S_2/NF was served as self-standing supercapacitor electrode. The optimized PANI/Ni_3S_2/NF-100 electrode exhibits a high areal capacity of 1.56 mA h cm^{-2} (487.5 mA h g^{-1}) at 5 mA cm^{-2} and good rate capability (57.7% retention at 50 mA cm^{-2}), which significantly outperforms individual PANI/NF or Ni_3S_2/NF. Furthermore, an asymmetric supercapacitor fabricated by PANI/Ni_3S_2/NF-100 and activated carbon electrodes can deliver a high energy density of 48.3 W h kg^{-1} at a power density of 799.8 W kg^{-1} with outstanding durability (85.7% retention of the initial capacity) during 15000 consecutive charge-discharge cycles. The superior electrochemical performance of PANI/Ni_3S_2/NF-100 is attributed to the unique hierarchical PANI/Ni_3S_2 nanosheet arrays structure. Firstly, the hierarchical open network facilitates the electrolyte ions transport. Secondly, the ultrathin 2D Ni_3S_2 nanosheets lead to abundant electroactive sites for the Faradaic process, and the conductive PANI layer builds superb highway for fast electron transfer. Thirdly, the free-standing electrode enables fast redox reaction and low interfacial resistance. Finally, the synergetic effect of Ni_3S_2 and PANI also contributes to the enhanced capacity.

1. Introduction

With the rapid consumption of fossil energy worldwide, the demand for green and sustainable energy is becoming more and more urgent.[1] Efficient and convenient energy storage systems can effectively expand the application of renewable energy, and greatly reduce the waste of energy. Therefore, exploring efficient and reliable energy conversion and storage devices has aroused great research interest. Supercapacitors (SCs), also named electrochemical capacitors, which are green and environmentally friendly. SCs have been the focus of researchers since inception because of their fast charge delivery capability, high cycling stability and large power density.[2] However, for practical applications, the energy density of SCs is still unsatisfactory. Electrode material is the core of SCs, which directly determines the comprehensive performance of SCs. In this circumstance, many efforts have been done to explore and design advanced electrode materials to meet various requirements of SCs.

Recently, transition metal sulfide compounds, such as CoS,[3] Ni_3S_2,[4] MnS,[5] MoS[6] and so on have been widely explored for SCs owing to high theoretical capacity and abundant oxidation states for redox reactions. Compared with powder transition metal sulfides, transition metal sulfide nanostructures grown in situ on conductive substrates have faster electron transfer rates and larger active surface areas, leading to better electrochemical performance. For example, Han and co-workers designed a porous Co_9S_8 nanosheets array, and it exhibited a high specific capacitance of 1098.8 F g^{-1} at 0.5 A g^{-1} with good rate capability and cycling stability.[7] Huang et al. have prepared a Ni–Zn–Co–S nanoarray, which displayed high areal capacity (1.11 mA h cm^{-2} at 10 mA cm^{-2}) and moderate capacity retention (85% after 1000 cycles).[8] However, since the slow reaction kinetics and relatively low electrical conductivity, the activity, rate capacity and cyclic stability of these metal sulfide arrays are still unsatisfactory.

Conductive polymer, as a kind of electrode materials, has aroused great research interest owing to its high conductivity and low price. The good wettability arising from the abundant hydrophilic functional groups of conductive polymer makes it

[a] Q. Cheng, Prof. L. Han, Prof. K. Tao
State Key Laboratory Base of Novel Functional Materials and Preparation Science
School of Materials Science & Chemical Engineering
Ningbo University
Ningbo, Zhejiang 315211, P.R. China
E-mail: taokai@nbu.edu.cn
hanlei@nbu.edu.cn
[b] C. Yang
Institute of Drug Discovery Technology
Ningbo University
Ningbo, Zhejiang 315211, P.R. China
E-mail: yangcui@nbu.edu.cn
[c] Prof. L. Han, Prof. K. Tao
Key Laboratory of Photoelectric Materials and Devices of Zhejiang Province
Ningbo University
Ningbo, Zhejiang 315211, P.R. China
[d] Prof. L. Han, Prof. K. Tao
State Key Laboratory of Structural Chemistry
Fujian Institute of Research on the Structure of Matter, Chinese Academy of Sciences
Fuzhou, Fujian 350002, PR China

Supporting information for this article is available on the WWW under https://doi.org/10.1002/batt.201900221

This publication is part of a joint Special Issue with ChemSusChem focusing on "2D Energy Storage Materials"

easier for electrolyte ions to enter and to diffuse rapidly.[9] Therefore, combining the transition metal sulfides with the conductive polymer material will lead to the enhanced electrochemical activity, demonstrating an effective way of fabricating high-performance electrode materials for SCs.

Herein, inspired by the above ideas, we report an effective multi-step approach to fabricate hierarchical polyaniline (PANI)/Ni_3S_2 nanosheet arrays on Ni foam (PANI/Ni_3S_2/NF). Firstly, the 2D Ni–MOF nanosheet arrays are directly used as the precursor and template to obtain Ni3S2 through a facile hydrothermal sulfidation process. Then, the PANI nanoflakes are grown on the top of Ni_3S_2/NF by the electrodeposition method. The optimized PANI/Ni_3S_2/NF-100 electrode exhibits excellent electrochemical performance, delivering a high areal capacity of 1.56 mA h cm^{-2} (487.5 mA h g^{-1}) at 5 mA cm^{-2} with good rate capability (retention of 57.7% at 50 mA cm^{-2}). Besides, an asymmetric supercapacitor (ASC) assembled from PANI/Ni_3S_2/NF-100 and activated carbon (AC) electrodes can output a high energy density of 48.3 W h kg^{-1} at a power density of 799.8 W kg^{-1} with excellent electrochemical durability (retention of 85.7% after 15000 cycles at 5 A g^{-1}), outperforming many other related ASC devices.

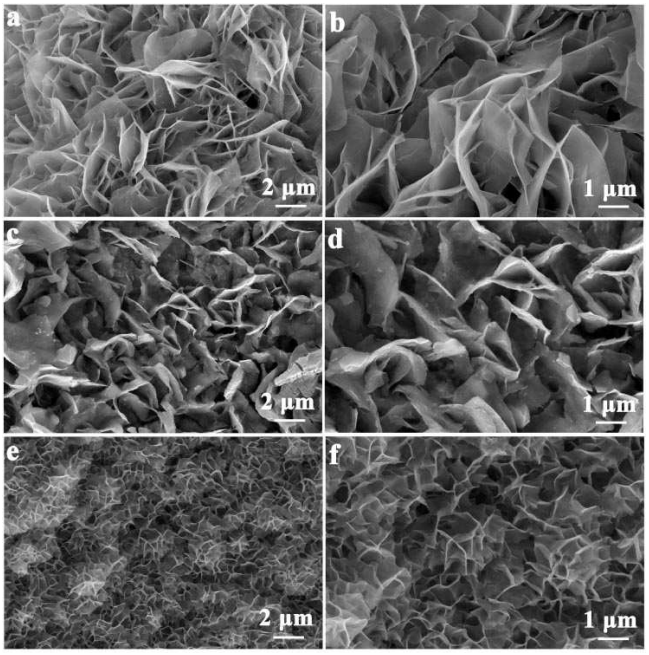

Figure 1. SEM images of (a, b) Ni–MOF/NF, (c, d) Ni_3S_2/NF and (e,f) PANI/Ni_3S_2/NF-100 at low and high magnifications.

2. Results and Discussion

Scheme 1 illustrates the synthesis of PANI/Ni_3S_2/NF. Firstly, Ni^{2+} and H_2BDC were assembled into ultrathin Ni–MOF nanosheets on NF through a hydrothermal process at 125 °C for 12 h. Subsequently, the 2D Ni–MOF was sulfurized by thioacetamide (TAA) to obtain the Ni_3S_2. Finally, a layer of PANI nanoflakes was coated on the top of Ni_3S_2 by electrodeposition with different times.

The morphologies of the electrodes were investigated by SEM. As depicted Figure 1a and b, the ultrathin Ni–MOF nanosheets (18 nm) with smooth surfaces cover the NF substrate uniformly and densely. The interlaced nanosheets almost align perpendicularly to the NF substrate. After sulfurization with TAA at 120 °C for 4 h, the surfaces of the nanosheets (Figure 1c and d) become rough, and there are some nanoparticle attached on the surfaces, which is typical for metal sulfides.[7,10] Notably, the sulfurization does not alter the nanosheet arrays structure of Ni–MOF/NF. According to the cross-sectional view (Figure S1), the Ni_3S_2 nanosheet arrays display an average height about 2.6 μm. The SEM images of the PANI/Ni_3S_2/NF-100 are shown in Figure e and f, abundant interconnected PANI nanoflakes are uniformly deposited on the top of Ni_3S_2/NF, forming a hierarchical open network structure. The height of the nanosheet arrays increases to 3.3 μm (Figure S2), implying a layer of PANI nanoflakes has been successfully deposited. This unique hierarchical structure can increase the accessible surface area and can expose more electrochemically active sites. In the meantime, it provides rapid pathway for electrolyte ions, contributing to an enhancement of electrochemical performance.[11] It is noteworthy that the structure of the composite electrode can be tailored by changing the electrodeposition time, as shown in Figure S3. The hierarchical nanosheets array structures with open networks are obtained for PANI/Ni_3S_2/NF-50 (Figure S3a and S3ab) and PANI/Ni_3S_2/NF-100 (Figure 1e and f). However, the PANI nanoflakes become crowed (Figure S3c and S3d) for PANI/Ni_3S_2/NF-150, and the open network collapses when the electrodeposition time is extended to 200 s (Figure S3e and S3 f).

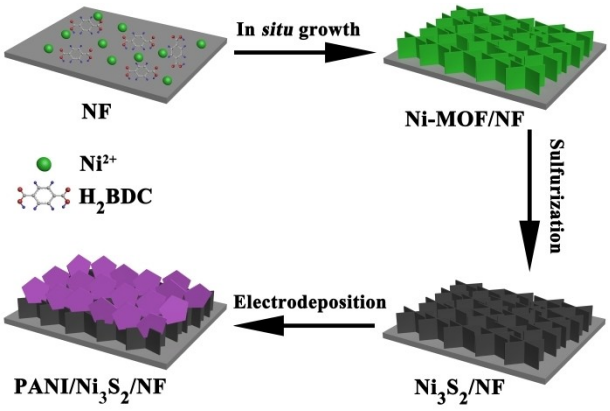

Scheme 1. Illustration showing the synthesis of PANI/Ni_3S_2/NF.

The compositional and structural properties of the PANI/Ni_3S_2/NF-100 sample were further revealed by TEM. The hierarchical nanosheets structure is unambiguously observed in Figure 2a. A closer observation in Figure 2b indicates that the Ni_3S_2 nanosheets are ultrathin. The high-resolution TEM (HRTEM) image of PANI/Ni_3S_2/NF-100 (Figure 2c) displays the obvious lattice fringes with spacing of 0.20 nm, matching well with the (202) plane of Ni_3S_2 (PDF#76-1870). The selected area electron diffraction (SAED) pattern (inset of Figure 2c) suggests

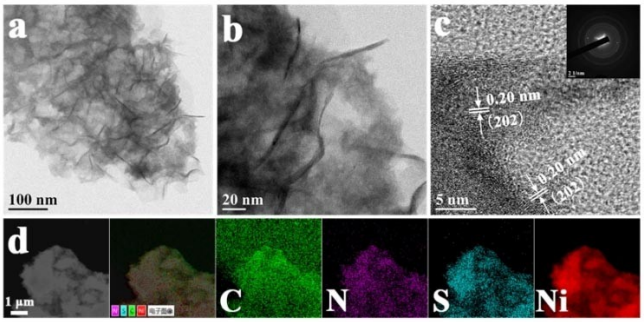

Figure 2. (a,b) TEM images, (c) HRTEM, and (d) STEM image and elemental mappings of PANI/Ni_3S_2/NF-100s. Inset of (c): SAED pattern.

the polycrystalline nature of the PANI/Ni_3S_2/NF-100. STEM image and EDS mappings (Figure 2d) reveal the uniform distribution of C, N, S and Ni elements over the sample, implying the successful preparation of hierarchical PANI/Ni_3S_2 nanosheet arrays.

XRD patterns of the Ni_3S_2/NF and PANI/Ni_3S_2/NF-100 samples are shown in Figure 3a. The main diffraction peaks at $2\theta = 22.1$, 31.4, 38.1, 44.7, 50.3 and 55.4° are indexed to the (101), (110), (003), (202), (113), (211), (122) and (300) planes of the heazlewoodite phase of Ni_3S_2 (PDF#76-1870), whereas the peaks at $2\theta = 44.7$, 52.1 and 76.7° belong to metallic Ni (PDF#04-0850) from NF substrate.[12] Compared with Ni_3S_2/NF electrode, the PANI/Ni_3S_2/NF-100 electrode shows slightly decreased Ni_3S_2 diffraction peaks probably because that the Ni_3S_2 nanosheets are covered by PANI nanoflakes layer. There are no diffraction peaks that can be ascribed to PANI due to the amorphous feature of the PANI layer.[13] The surface chemical compositions and valence states of the PANI/Ni_3S_2/NF-100 were analyzed by XPS. The survey spectrum in Figure 3b reveals the presence of Ni, S, C, and N elements in PANI/Ni_3S_2/NF-100 sample. The Ni 2p spectrum (Figure 3c) was fitted with two bands with two shake-up satellites. The peak at 856.0 eV (Ni $2p_{3/2}$) is ascribed to Ni^{2+} and the binding energy at 873.6 eV (Ni $2p_{1/2}$) is indexed to Ni^{3+}.[11,14] The S 2p spectrum (Figure 3d) presents two bands at 163.7 (S $2p_{3/2}$) and 164.5 eV (S $2p_{1/2}$), suggesting the existence of S^{2-} in Ni_3S_2. Moreover, the satellite peak at 168.8 eV is ascribed to the high oxidation state sulfur, arising from the oxidation of surface S.[15] The high-resolution XPS spectrum of C 1s (Figure 3e) displays three distinct binding energies around 284.6, 285.6 and 288.9 eV correspond to C–C, C–N/C–S and C=O, respectively.[16] The N 1s spectrum (Figure 3f) showing a peak at 399.0 eV signifies the amino group (–NH–) in benzenoid amine or amide groups, indicating the existence of PANI.[11]

The as-prepared nanosheet arrays were directly applied as working electrodes for SCs. Figure 4a presents the CV curves of Ni_3S_2/NF, PANI/NF and PANI/Ni_3S_2/NF hybrid electrodes with different electrodeposition times (50, 100, 150 and 200 s) at a scan rate of 30 mV s^{-1} within the potential window of −0.1–0.8 V (vs. SCE). The distinct redox peaks are observed, implying the charge storage is controlled by Faradaic process.[17] The

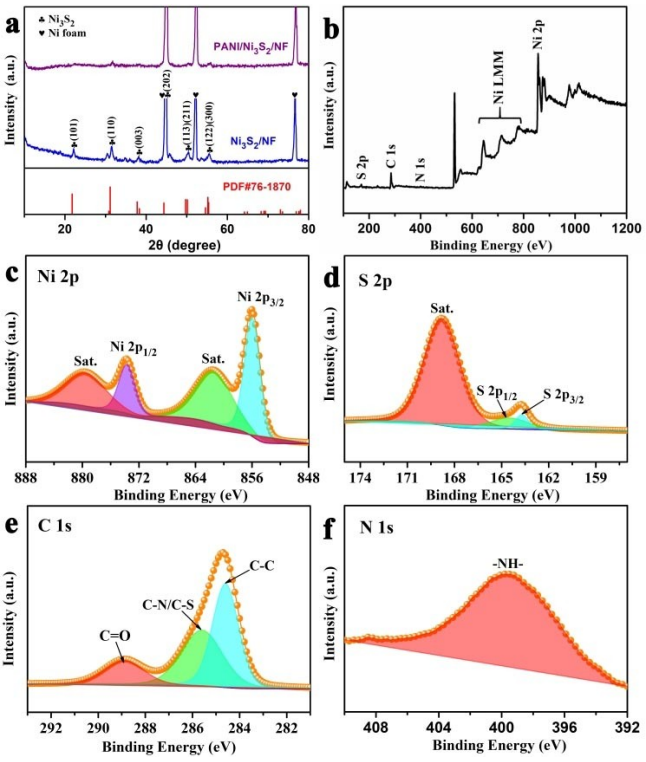

Figure 3. (a) XRD patterns of Ni_3S_2/NF and PANI/Ni_3S_2/NF and the XPS spectra of PANI/Ni_3S_2/NF-100: (b) survey; (c) Ni 2p; (d) S 2p; (e) C 1s and (f) N 1s.

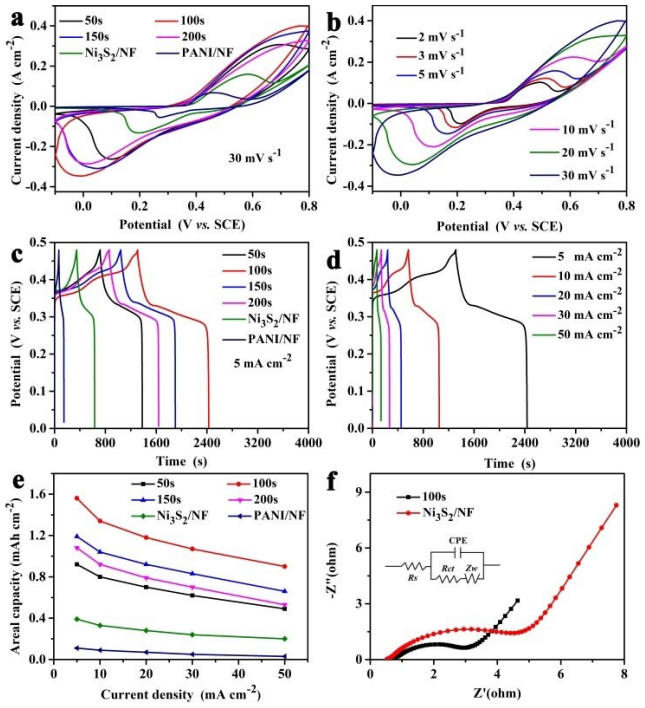

Figure 4. (a,c) Comparative CV and GCD curves of the Ni_3S2/NF, PANI/NF and PANI/Ni_3S_2/NF hybrid electrodes with various electrodeposition times. (b,d) CV and GCD curves of PANI/Ni_3S_2/NF-100. (e) Specific areal capacity of Ni_3S_2/NF, PANI/NF and PANI/Ni_3S_2/NF hybrid electrodes with various electrodeposition times. (f) Nyquist plots of Ni_3S_2/NF and PANI/Ni_3S_2/NF-100.

redox peaks arise from Ni–S/Ni–S–OH transformations, as described by Eq. (1):[18]

$$Ni_3S_2 + 3OH^- \leftrightarrow Ni_3S_2(OH)_3 + 3e^- \quad (1)$$

Obviously, the area enclosed by CV curve of PANI/Ni_3S_2/NF composite electrodes is much bigger than that of single Ni_3S_2/NF or PANI/NF electrode, suggesting that the deposition a layer of PANI can significantly improve electrochemical activity. Moreover, of all these hybrid electrodes, PANI/Ni_3S_2/NF-100 electrode exhibits highest electrochemical activity. Figure 4b shows typical CV curves of PANI/Ni_3S_2/NF-100 with different scan rates from 2 to 30 mV s^{-1}. The shape of the CV curve is well kept as the scan rate rising, implying the excellent rate capability and reversibility of the electrode. The CV curves of the Ni_3S_2/NF, PANI/NF and PANI/Ni_3S_2/NF-n (50, 150 and 200) electrodes at various scanning rates are presented in Figure S4a, S5a, S6a, S7a and S8a. Figure 4c compares GCD curves of Ni_3S_2/NF, PANI/NF and PANI/Ni_3S_2/NF hybrid electrodes at 5 mA cm^{-2}. As expected, PANI/Ni_3S_2/NF-100 shows much longer charge/discharge time compared with other electrodes, implying it has the largest capacity. Figure 4d shows the GCD curves of the PANI/Ni_3S_2/NF-100 electrode in a voltage window of 0–0.48 V (vs. SCE) under different current density of 5–50 mA cm^{-2}. For comparison, the GCD curves of the Ni_3S_2/NF, PANI/NF and PANI/Ni_3S_2/NF-n (50, 150 and 200) electrodes are presented in Figure S4b, S5b, S6b, S7b and S8b. According to the GCD curves, the PANI/Ni_3S_2/NF-100 displays a high areal capacity of 1.56 mA h cm^{-2} at 5 mA cm^{-2} (Figure 4e), and the corresponding specific capacity is as high as 487.5 mA h g^{-1}. Notably, of all the electrodes, the PANI/Ni_3S_2/NF-100 exhibits highest capacity. Even at a high current density of 50 mA cm^{-2}, 57.7% of the capacity (5 mA cm^{-2}) can be retained, indicating the good rate capability of the PANI/Ni_3S_2/NF-100 electrode. The specific capacity of PANI/Ni_3S_2/NF-100 is comparable or superior to that of most of the nickel sulfide based electrode materials reported previously (see Table S1 for detailed comparison). The EIS measurements of Ni_3S_2/NF and PANI/Ni_3S_2/NF-100 were conducted in a frequency from 0.01 to 100 KHz with amplitude of 5 mV. The EIS data was fitted with an equivalent circuit, as shown in Figure 4f (inset). The Nyquist plots (Figure 4f) of Ni_3S_2/NF and PANI/Ni_3S_2/NF-100 electrodes are analogous, which are composed of a quasi-semicircle at higher frequencies and a straight oblique line at lower frequencies. The interception with real-axis at higher frequencies represents the series resistance (R_s) value, containing the electrolyte resistance, the inherent resistance of electrode material, and the contact resistance of active material and collector interface.[19] The radius of the semicircle corresponds to charge transfer impedance (R_{ct}),[20] while the slope of the oblique line is the Warburg resistance (Z_w) reflecting the diffusive impedance of OH^- within the electrode.[21] As shown in Figure 4f, the PANI/Ni_3S_2/NF-100 electrode has smaller radius of semicircle than that of Ni_3S_2/NF, demonstrating its lower charge-transfer impedance.[22] Therefore, the PANI/Ni_3S_2/NF-100 electrode possesses fast electron transport and good charge-transfer kinetics, which is consistent with the CV and GCD results aforementioned. The Nyquist plots of other PANI/Ni_3S_2/NF and PANI/NF are presented in Figure S9. The electrochemical data suggests that the introduction of a PANI layer can significantly improve the electrochemical performance of Ni_3S_2/NF. The high capacity of the PANI/Ni_3S_2/NF-100 electrode is ascribed to following aspects: (1) The hierarchical 3D open network facilitates the electrolyte ions diffusion.[23] (2) The ultrathin 2D Ni_3S_2 nanosheets can expose more electroactive sites for Faradaic reactions. Thus, the 2D Ni_3S_2 nanosheets exhibit significantly improved areal capacity compared with 3D nanoflowers derived from Ni–MOF (Figure S10 and S11). (3) The high conductive PANI layer builds superb highway for fast electron transfer.[24] (4) The direct growth of PANI/Ni_3S_2 on NF enables fast Faradaic reactions and high electronic conductivity.[25] The synergetic effect of 2D nanosheets structure, conductive PANI and high electrochemical activity of individual Ni_3S_2 and PANI contributes to the enhanced capacity.[26]

The electrochemical performance of PANI/Ni_3S_2/NF-100 was further evaluated in a two-electrode ASC device (Figure 5a), where PANI/Ni_3S_2/NF-100 and AC were cathode and anode, respectively. Judging from the CV (Figure S12a) and GCD (Figure S12b) curves, the AC electrode displays the typical EDLC characteristics. The CV curves (Figure S13) of individual PANI/Ni_3S_2/NF-100 and AC electrodes show stable voltage windows of −0.1–0.8 V and −1–0 V, respectively. The CV curves of the PANI/Ni_3S_2/NF-100//AC with different voltage windows from 1.4

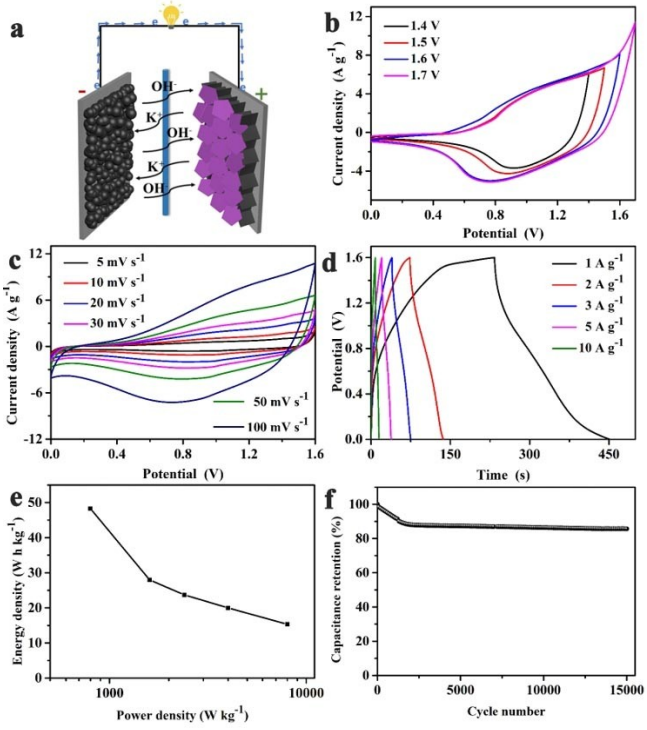

Figure 5. (a) Scheme illustrating the PANI/Ni_3S_2/NF-100//AC. (b) CV curves of the PANI/Ni_3S_2/NF-100//AC with various voltage windows at a scan rate of 50 mV s^{-1}. (c) CV curves of the ASC at various sweep rates. (d) GCD curves of the ASC at various current densities. (e) Ragone plots showing energy density and power density of the ASC. (f) Cycling performance of the ASC at a current density of 5 A g^{-1} for 15000 cycles.

to 1.7 V are shown in Figure 5b, where the ASC works stably at operating voltage window up to 1.6 V without polarization and oxygen evolution reaction. The CV curves of the PANI/Ni_3S_2/NF-100//AC working at 1.6 V are shown in Figure 5c. With the scan rates rise, the shape of CV curves is well kept, indicating good reversibility of the ASC. Figure 5d shows the GCD curves of the PANI/Ni_3S_2/NF-100//AC at different current densities. The specific capacity (Figure S14) of the ASC device is estimated to be 60.4 mA h g^{-1} at 1 A g^{-1}, on the basis of the total amount of the active materials. When the current density is increased to 10 A g^{-1}, the capacity decreases to 19.2 mA h g^{-1} due to relatively slow redox reaction kinetics at large current density. The Ragone plots in Figure 5e shows the power density and energy density of the ASC, which are determined by Eqs (4) and (5). Impressively, the ASC exhibits a maximum energy density of 48.3 W h kg^{-1} with a power density of 799.8 W kg^{-1} at 1 A g^{-1}. The ASC can still deliver an energy density of 15.34 W h kg^{-1} at a high power density of 8000.3 W kg^{-1}. Noteworthy, the high energy and power density of PANI/Ni_3S_2/NF-100//AC significantly outperforms those of relevant ASCs reported previously including Ni_3S_2@PPy/NF//AC (17.54 W h kg^{-1} at 179.33 W kg^{-1}),[27] neural network-like rGO/Ni_3S_2(rGO)/PP-PEFs//rGO/Ni/PP-PEFs (29.1 W h kg^{-1} at 0.54 kW kg^{-1}),[28] Ni_3S_2/CNFs//CNFs (25.8 W h kg^{-1} at 425 W kg^{-1}),[29] hierarchically structured Ni_3S_2/MWCNT-NC//AC (19.8 W h kg^{-1} at 798 W kg^{-1})[30] and 3D Ni_3S_2-rGO//AC (18.7 W h kg^{-1} at 124 W kg^{-1}).[31] Moreover, the cycling performance of the PANI/Ni_3S_2/NF-100//AC was evaluated by consecutive GCD processes (Figure 5f). The capacity of the ASC is stable with slight variation. Even after 15000 cycles, approximately 85.7% of the initial capacity is retained, indicating its high electrochemical durability. The SEM image of PANI/Ni_3S_2/NF-100 (Figure S15) after 15000 cycles shows that the nanosheet array is intact, further confirming its excellent stability.

3. Conclusions

We have demonstrated an effective multi-step method to fabricate hierarchical 2D PANI/Ni_3S_2 nanosheet arrays on Ni foam. The Ni_3S_2 nanosheet arrays were first synthesized by using a 2D Ni–MOF as the precursor and template through a facile hydrothermal sulfidation process. And then, PANI nanoflakes were deposited on the top of Ni_3S_2 nanosheets via electrodeposition method to form the hierarchical 3D open network structure. The optimized PANI/Ni_3S_2/NF-100 electrode exhibits best electrochemical performance, delivering a high areal capacity of 1.56 mA h cm^{-2} (487.5 mA h g^{-1}) at 5 mA cm^{-2} and a high rate capability of 57.7% at 50 mA cm^{-2}. Besides, an ASC based on PANI/Ni_3S_2/NF-100 and AC electrodes demonstrates a high energy density of 48.3 W h kg^{-1} with a power density of 799.8 W kg^{-1}, outperforming many other relevant ASCs. Moreover, the ASC displays excellent electrochemical durability in that 85.7% of the initial capacity can be retained during 15000 cycles of GCD tests. This work provides an effective approach for rational design of hierarchical electrodes for efficient electrochemical energy storage systems.

Experimental Section

Materials

1, 4-Benzenedicarboxylic acid (H_2BDC) was purchased from TCI Chemicals. Nickel chloride ($NiCl_2 \cdot 6H_2O$), thioacetamide (TAA), aniline and sulphuric acid were analysis grade and used as received. The NF substrate (2 cm × 3 cm) was cleaned thoroughly by ethanol and H_2O with sonication to remove oxide layer and impurities.

Synthesis of Ni_3S_2/NF nanosheet arrays

The Ni_3S_2 nanosheet arrays were synthesized by sulfidation of Ni–MOF nanosheet arrays (Ni–MOF/NF), which were synthesized according to our previous work.[32] The obtained Ni–MOF/NF was put in an autoclave containing TAA (0.04 M, ethanol). The autoclave was maintained at 120 °C for 6 h. Finally, the Ni_3S_2/NF was rinsed thoroughly with ethanol and dried. The amount of Ni_3S_2 on NF was estimated to be about 1.8 mg·cm^{-2} by weighing the NF before and after the deposition of Ni_3S_2.

Synthesis of PANI/Ni_3S_2/NF

The PANI layer was electrodeposited on the surface of Ni_3S_2/NF in a three-electrode cell containing aniline (0.1 M) and H_2SO_4 (1 M) under a constant voltage of 1.0 V, where Ni_3S_2/NF was employed as the working electrode. Ag/AgCl and Pt foil acted as the reference and counter electrodes, respectively. A series of PANI/Ni_3S_2/NF-n (n: electrodeposition time) electrodes with various electrodeposition time from 50 to 200 s were prepared. For comparison, the PANI layer was electrodeposited on NF (PANI/NF) by the same procedure used for PANI/Ni_3S_2/NF except for using bare NF as the substrate. The mass density of PANI was around 1.4 mg·cm^{-2}.

Characterization

The compositional and structural properties of the electrodes were analysed by X-ray diffraction (XRD), field emission scanning electron microscopy (FESEM), transmission electron microscopy (TEM), energy dispersive X-ray spectrometer (EDS) and X-ray photoelectron spectroscopy (XPS).

Electrochemical tests

The experiment was conducted by a three-electrode cell, where the as-fabricated nanosheet arrays were acted as the working electrode, a Pt foil was used as the counter electrode, and a saturated calomel electrode (SCE) was employed as the reference electrode. Cyclic voltammetry (CV), galvanostatic charge-discharge (GCD) and electrochemical impedance spectroscopy (EIS) analysis were conducted by an electrochemical workstation (Chenhua CHI 660E) in 2 M KOH. The areal capacity was calculated by Equation (2) as follows:

$$C_a = \frac{I \times \Delta t}{3600S} \quad (2)$$

where C_a (mA h cm^{-2}), I (mA), Δt (s) and S (cm^2) represented the areal specific capacity, constant current, discharge time and area of the electrode material, respectively.

The ASC was assembled by PANI/Ni_3S_2/NF-100 (anode) and AC (cathode) in 2 M KOH. The specific capacity, energy density and

power density of the PANI/Ni_3S_2/NF-100//AC ASC were evaluated by following Equations (3)–(5):

$$C_s = \frac{I \times \Delta t}{3.6m} \quad (3)$$

$$E = \frac{C \times (\Delta V)^2}{2 \times 3.6} \quad (4)$$

$$P = \frac{3600E}{\Delta t} \quad (5)$$

where C_s ($mA\,h\,g^{-1}$) was the specific capacity of ASC, I (A) was the discharge current, m (g) referred to the total amount of active materials on anode and cathode, Δt (s) was the full discharge time, ΔV (V) was the potential window, E ($W\,h\,kg^{-1}$) was the energy density, and P ($W\,kg^{-1}$) was the power density.

Acknowledgements

We thank the NSF of Zhejiang Province (LY20E020005), the NSFC (51572272 and 21971131), the NSF of Ningbo (2019 A610003), Open Foundation of State Key Laboratory of Structural Chemistry (20200022), the Foundation of State Key Laboratory of High-efficiency Utilization of Coal and Green Chemical Engineering (2018-K06) and the K.C. Wong Magna Fund in Ningbo University for financial support.

Keywords: PANI · Ni_3S_2 · nanosheet arrays · 2D MOF · supercapacitor

[1] a) Z. Huang, J. Song, L. Pan, X. Zhang, L. Wang, J. Zou, *Adv. Mater.* **2015**, *27*, 5309–5327; b) J. Zhang, Z. Zhao, Z. Xia, L. Dai, *Nat. Nanotechnol.* **2015**, *10*, 444–452; c) Q. Wu, M. Chen, K. Chen, S. Wang, C. Wang, G. Diao, *J. Mater. Sci.* **2015**, *51*, 1572–1580; d) S. Zheng, X. Li, B. Yan, Q. Hu, Y. Xu, X. Xiao, H. Xue, H. Pang, *Adv. Energy Mater.* **2017**, *7*, 1602733–1602759; e) D. Zhu, C. Guo, J. Liu, L. Wang, Y. Du, S. Z. Qiao, *Chem. Commun.* **2017**, *53*, 10906–10909; f) Y. Xu, S. Zheng, H. Tang, X. Guo, H. Xue, H. Pang, *Energy Storage Mater.* **2017**, *9*, 11–30.
[2] a) Y. Shao, M. El-Kady, J. Sun, Y. Li, Q. Zhang, M. Zhu, H. Wang, B. Dunn, R. Kaner, *Chem. Rev.* **2018**, *118*, 9233–9280; b) Q. Xue, J. Sun, Y. Huang, M. Zhu, Z. Pei, H. Li, Y. Wang, N. Li, H. Zhang, C. Zhi, *Small* **2017**, *13*, 1701827–1701837; c) K. Tao, X. Han, Q. Cheng, Y. Yang, Z. Yang, Q. Ma, L. Han, *Chem. Eur. J.* **2018**, *24*, 12584–12591.
[3] Z. Jiang, W. Lu, Z. Li, K. Ho, X. Li, X. Jiao, D. Chen, J. Mater, *Chem. A* **2014**, *2*, 8603–8606.
[4] L. Chen, L. Guan, J. Tao, *J. Mater. Sci.* **2019**, *54*, 12737–12746.
[5] T. Chen, Y. Tang, Y. Qiao, Z. Liu, W. Guo, J. Song, S. Mu, S. Yu, Y. Zhao, F. Gao, *Sci. Rep.* **2016**, *6*, 23289–23297.
[6] Y. Yang, H. Fei, G. Ruan, C. Xiang, J. M. Tour, *Adv. Mater.* **2014**, *26*, 8163–8168.
[7] X. Han, K. Tao, D. Wang, L. Han, *Nanoscale* **2018**, *10*, 2735–2741.
[8] Y. Huang, L. Quan, T. Liu, Q. Chen, D. Cai, H. Zhan, *Nanoscale* **2018**, *10*, 14171–14181.
[9] X. He, Y. Zhao, R. Chen, H. Zhang, J. Liu, Q. Liu, D. Song, R. Li, J. Wang, *ACS Sustainable Chem. Eng.* **2018**, *6*, 14945–14954.
[10] Y. J. Yang, Q. X. Ma, L. Han, K. Tao, *Inorg. Chem. Front.* **2019**, *6*, 1398–1404.
[11] L. Zhou, X. Zhang, D. Zheng, W. Xu, J. Liu, X. Lu, J. Mater, *Chem. A* **2019**, *7*, 10629–10635.
[12] Z. Li, W. Niu, Z. Yang, N. Zaman, W. Samarakoon, M. Wang, A. Kara, M. Lucero, M. V. Vyas, H. Cao, H. Zhou, G. E. Sterbinsky, Z. Feng, Y. Du, Y. Yang, *Energy Environ. Sci.*, doi:10.1039/C9EE02657F.
[13] X. G. Li, A. Li, M. R. Huang, *Chemistry* **2008**, *14*, 10309–10317.
[14] G. Wang, Z. Yang, Y. Du, Y. Yang, *Angew. Chem. Int. Ed.* **2019**, *58*, 15848–15854.
[15] a) Y. L. Wang, X. Q. Wei, M. B. Li, P. Y. Hou, X. J. Xu, *Appl. Surf. Sci.* **2018**, *436*, 42–49; b) J. Zhao, B. Guan, B. Hu, Z. Xu, D. Wang, H. Zhang, *Electrochim. Acta* **2017**, *230*, 428–437; c) L. Guo, Z. Yang, K. Marcus, Z. Li, B. Luo, L. Zhou, X. Wang, Y. Du, Y. Yang, *Energy Environ. Sci.* **2018**, *11*, 106–114.
[16] W. Shuang, H. Huang, L. Kong, M. Zhong, A. Li, D. Wang, Y. Xu, X.-H. Bu, *Nano Energy* **2019**, *62*, 154–163.
[17] a) Y. M. Chen, Z. Li, X. W. Lou, *Angew. Chem. Int. Ed. Engl.* **2015**, *54*, 10521–10524; b) H. Chen, J. Jiang, L. Zhang, H. Wan, T. Qi, D. Xia, *Nanoscale* **2013**, *5*, 8879–8883.
[18] a) K. Krishnamoorthy, G. K. Veerasubramani, S. Radhakrishnan, S. J. Kim, *Chem. Eng. J.* **2014**, *251*, 116–122; b) X. Li, J. Rong, B. Wei, *ACS Nano* **2010**.
[19] Y. Zhao, X. He, R. Chen, Q. Liu, J. Liu, J. Yu, J. Li, H. Zhang, H. Dong, M. Zhang, J. Wang, *Chem. Eng. J.* **2018**, *352*, 29–38.
[20] X. Li, L. Wang, J. Shi, N. Du, G. He, *ACS Appl. Mater. Interfaces* **2016**, *8*, 17276–17283.
[21] X. Xia, Z. Zeng, X. Li, Y. Zhang, J. Tu, N. C. Fan, H. Zhang, H. J. Fan, *Nanoscale* **2013**, *5*, 6040–6047.
[22] M. Yan, Y. Yao, J. Wen, L. Long, M. Kong, G. Zhang, X. Liao, G. Yin, Z. Huang, *ACS Appl. Mater. Interfaces* **2016**, *8*, 24525–24535.
[23] W. Xiong, X. Hu, X. Wu, Y. Zeng, B. Wang, G. He, Z. Zhu, J. Mater, *Chem. A* **2015**, *3*, 17209–17216.
[24] a) S. C. P. Baig E, S. Pillai, M. C. Aravind, S. J. Devaki, *Electrochim. Acta* **2019**, *324*; b) Z. Yang, J. Ma, B. Bai, A. Qiu, D. Losic, D. Shi, M. Chen, *Electrochim. Acta* **2019**, *322*.
[25] J. S. Lee, D. H. Shin, W. Kim, J. Jang, J. Mater, *Chem. A* **2016**, *4*, 6603–6609.
[26] a) L. Ma, H. Fan, X. Wei, S. Chen, Q. Hu, Y. Liu, C. Zhi, W. Lu, J. A. Zapien, H. Huang, J. Mater, *Chem. A* **2018**, *6*, 19058–19065; b) Q. H. Gong, Y. J. Li, H. Huang, J. Zhang, T. T. Gao, G. W. Zhou, *Chem. Eng. J.* **2018**, *344*, 290–298.
[27] L. Long, Y. Yao, M. Yan, H. Wang, G. Zhang, M. Kong, L. Yang, X. Liao, G. Yin, Z. Huang, *J. Mater. Sci.* **2016**, *52*, 3642–3656.
[28] N. Wang, G. Han, Y. Chang, W. Hou, Y. Xiao, H. Li, *Electrochim. Acta* **2019**, *317*, 322–332.
[29] L. Yu, L. Zhang, H. B. Wu, X. W. Lou, *Angew. Chem. Int. Ed.* **2014**, *53*, 3711–3714; *Angew. Chem.* **2014**, *126*, 3785–3788.
[30] C. S. Dai, P. Y. Chien, J. Y. Lin, S. W. Chou, W. K. Wu, P. H. Li, K. Y. Wu, T. W. Lin, *ACS Appl. Mater. Interfaces* **2013**, *5*, 12168–12174.
[31] F. Cai, R. Sun, Y. Kang, H. Chen, M. Chen, Q. Li, *RSC Adv.* **2015**, *5*, 23073–23079.
[32] Q. Cheng, K. Tao, X. Han, Y. Yang, Z. Yang, Q. Ma, L. Han, *Dalton Trans.* **2019**, *48*, 4119–4123.

Manuscript received: December 19, 2019
Revised manuscript received: January 17, 2020
Accepted manuscript online: January 21, 2020
Version of record online: January 29, 2020